Dioxygen and Carbon Monoxide Uptake by Iridium(I) Complexes Stabilized by Mixed N,P-Donor Ligands

Pierluigi Barbaro,[†] Claudio Bianchini,*[,†] Franco Laschi,[‡] Stefano Midollini,[†] Simonetta Moneti,[†] Giancarlo Scapacci,[†] and Piero Zanello[‡]

Istituto per lo Studio della Stereochimica ed Energetica dei Composti di Coordinazione del CNR, Via J. Nardi 39, 50132 Firenze, Italy, and Dipartimento di Chimica, Università di Siena, Pian dei Mantellini 44, 53100 Siena, Italy

Received May 7, 1993[⊗]

The preparation of a new family of iridium(I) complexes with the mixed-donor bidentate ligands *o*-$Ph_2PC_6H_4$-CH=NR (PNalkyl) (R = Et, Pr^i, Bu^t) is described. In these complexes, the iridium center is coordinated by two PNalkyl ligands in a square-planar environment. All $[(PNalkyl)_2Ir]^+$ compounds undergo reversible electron transfer to the Ir(0) oxidation state as well as irreversible oxidation to Ir(III). Only for R = Bu^t is the Ir(II) oxidation state accessible through a reversible oxidation process. For comparative purposes, the electrochemical behavior of the Rh(I) congeners $[(PNalkyl)_2Rh]PF_6$ has been investigated. Illustrative examples of the paramagnetic Ir(0), Rh(0), Ir(II), and Rh(II) derivatives have been studied by ESR spectroscopy, which confirms that the unpaired electron is mainly localized on the metal center. The Ir(I) complexes $[(PNalkyl)_2Ir]Y$ (Y = BPh_4^-, PF_6^-, Cl^-; alkyl = Et, Pr^i) react with O_2, in organic solvent solutions at room temperature, to form peroxo complexes of formula $[(PNalkyl)_2Ir(O_2)]Y$. The molecular structure of the PNEt derivative $[(PNEt)_2(O_2)]PF_6$ has been determined by X-ray diffraction methods: monoclinic $P2_1/a$, a = 17.426(4) Å, b = 14.685(3) Å, c = 16.131(4) Å, α = 90.00(0)°, β = 98.07(2)°, γ = 90.00(0)°, Z = 4, R = 0.053. The O–O bond distance is 1.47(1) Å. The coordination of the metal may alternatively be described as distorted trigonal bipyramidal or distorted octahedral, according to whether the dioxygen molecule is treated as occupying one or two equatorial sites, respectively. The steric hindrance of the alkyl substituent on the imino donors appears as a limiting factor for the dioxygen uptake, as shown by the fact that $[(PNBu^t)_2Ir]^+$ does not react with O_2. Unlike the rhodium congeners, the Ir(I) complexes do not behave as oxygen carriers, the O_2 molecule being irreversibly coordinated to the metal center even at high temperature. In contrast, reversible square-pyramidal adducts form upon reaction of the PNEt and PNPr^i Ir(I) complexes with CO. No reaction occurs with the PNBu^t derivative, confirming that the size of the imino substituent controls the access of incoming reagents at the metal center.

Introduction

The uptake of dioxygen by transition metal complexes is a reaction which has considerable significance in chemistry and aereobic biology.[1,2] The subject has extensively been reviewed,[3] but it is still a challenge to understand the molecular details and mechanism for the dioxygen uptake and transport by metal complexes.

In a previous paper, some of us reported the reactivity of some square-planar Rh(I) complexes with the bidentate ligands *o*-$Ph_2PC_6H_4CH$=NR (R = Et, Pr^n, Pr^i, Bu^t) (PNalkyl) toward dioxygen.[4] With the exception of the PNBu^t complex, which does not react with O_2, all Rh(I) complexes $[(PNalkyl)_2Rh]^+$ are efficacious oxygen carriers.

Our next step was to replace rhodium with other transition metals in order to gain insight into the role played by the nature of the metal in the dioxygen uptake and transport while maintaining the overall complex framework. We report here the results for iridium.

Helpful to our study of the reactions with O_2 was an investigation of the electron-transfer properties of the starting Ir(I) and Rh(I) complexes of formula $[(PNalkyl)_2M]^+$. Besides providing information on the mechanism of the O_2 uptake, the electrochemical study has allowed us to generate uncommon examples of mononuclear rhodium and iridium complexes with a d^7 electronic configuration, which have been characterized by X-band ESR spectroscopy.

Experimental Section

Materials and Methods. Unless otherwise stated, all manipulations were performed under a nitrogen atmosphere. Acetone and *n*-heptane were distilled over K_2CO_3 and Na, respectively. All the other chemicals were commercial products and were used as received without further purification. $[Ir(COE)_2Cl]_2$[5] (COE = cyclooctene) and the ligands *o*-$Ph_2PC_6H_4CH$=NR (R = Et (PNEt), Pr^i (PNPr^i), Bu^t (PNBu^t)) were prepared according to literature methods.[4] $[(PNEt)_2Rh]PF_6$ (**4b**$^+$), $[(PNPr^i)_2Rh]PF_6$ (**5b**$^+$), and $[(PNBu^t)_2Rh]PF_6$ (**6b**$^+$) were prepared as previously described.[4] The solid compounds were collected on sintered-glass frits and washed with *n*-pentane before being dried in a stream of nitrogen. Infrared spectra were recorded on a Perkin-Elmer 1600 Series FT-IR spectrometer using samples mulled in Nujol between KBr plates. Proton NMR spectra were recorded at 200.133 MHz on a Bruker 200-ACP spectrometer. Chemical shifts are relative to tetramethylsilane as external reference or calibrated against the solvent as the reference signal. $^{31}P\{^1H\}$ NMR spectra were recorded on a Bruker 200-ACP spectrometer operating at 81.015 MHz. Chemical shifts are relative to external 85% H_3PO_4 with downfield values reported as positive. Conductivities were

[†] Istituto per lo Studio della Stereochimica ed Energetica dei Composti di Coordinazione del CNR.

[‡] Università di Siena.

[⊗] Abstract published in *Advance ACS Abstracts,* March 15, 1994.

(1) Sawyer, D. T. *Oxygen Chemistry*; Oxford University Press: New York, 1991.

(2) Sawyer, D. T. *CHEMTECH* **1988**, *18*, 369.

(3) (a) Allen, H.; Hill, O. Dioxygen, Superoxide and Peroxide. In *Comprehensive Coordination Chemistry*; Wilkinson, G., Gillard, R. D., McCleverty, J. A., Eds.; Pergamon Press: Oxford, England, 1987; Vol. 2, p 315. (b) *Oxygen Complexes and Oxygen Activation by Transition Metals*; Martell, A. E., Sawyer, D. T., Eds.; Plenum Press: New York, 1988. (c) Mimoun, H. Metal Complexes in Oxidation. In *Comprehensive Organometallic Chemistry*; Wilkinson, G., Stone, F. G. A., Abel, E. W., Eds.; Pergamon Press: Oxford, England, 1982; Vol. 6, p 317. (d) Drago, R. S. *Coord. Chem. Rev.* **1992**, *117*, 185. (e) *Metal Ion Activation of Dioxygen*, Spiro, T. G., Ed.; Wiley: New York, 1980. (f) Vaska, L. *Acc. Chem. Res.* **1976**, *9*, 175. (g) Valentine, J. S. *Chem. Rev.* **1973**, *73*, 235.

(4) Ghilardi, C.; Midollini, S.; Moneti, S.; Orlandini, A.; Scapacci, G. *J. Chem. Soc., Dalton Trans.* **1992**, 3371.

(5) Herde, J. L.; Lambert, J. C.; Senoff, C. V. *Inorg. Synth.* **1974**, *15*, 18.

0020-1669/94/1333-1622$04.50/0

Scheme 1

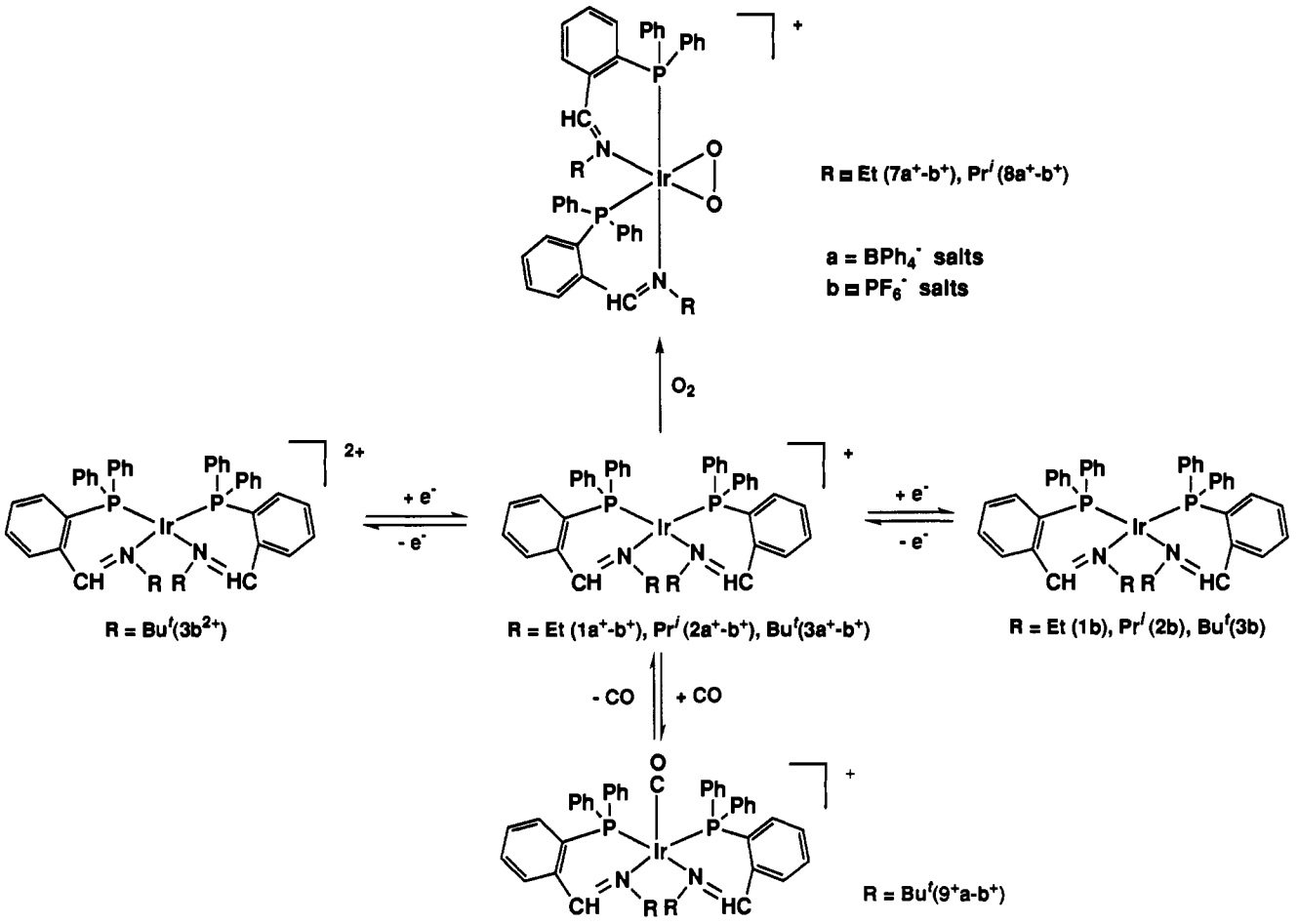

measured with a Model 990101 Orion conductance cell connected to a Model 101 conductivity meter. The conductivity data were obtained at sample concentrations of ca. 10^{-3} M in acetone solutions at room temperature. The materials and the apparatus used for the electrochemical experiments have been described elsewhere.[6a] Direct current voltammograms at a platinum electrode with periodical renewal of the diffusion layer (DCV) have been obtained as previously described.[6b] When necessary, deareation of solutions was performed by bubbling argon for 15 min. Unless otherwise stated, the potential values are relative to an aqueous calomel electrode (SCE) and refer to a controlled temperatures (see text). Low-temperature macroelectrolysis tests were performed by using the Ag/AgCl reference electrode, the potential of which was –0.04 V *vs* SCE. Under the present experimental conditions, the ferrocenium/ferrocene couple was located at +0.46 and +0.45 V in acetone and dichloromethane solutions, respectively. X-Band ESR spectra were recorded with an ER 200 D-SRC Bruker spectrometer operating at ω_0 = 9.78 GHz. The operational microwave frequency (Bruker Microwave Bridge ER 041 MR) was tested with an XL 3120 microwave frequency counter. The control of the external magnetic field was obtained with a microwave bridge ER 041 MR Bruker wavemeter. The temperature was varied and controlled with an ER 4111 VT Bruker device with an accuracy of ±1 °C. In order to estimate accurate g_{iso} and g_{aniso} values over the temperature range of interest, the diphenylpicrylhydrazyl free radical (DPPH) was used as the H_0 external magnetic field marker (g_{iso}(DPPH) = 2.0036). In order to ensure quantitative reproducibility, the samples were placed into calibrated quartz capillary tubes permanently positioned in the resonance cavity. Photochemical reactions were performed by using a Helios Italquartz UV BF apparatus. The photolysis source was a 135-W (principal emission wavelength 366 nm) high-pressure mercury vapor immersion lamp equipped with a water filter to remove excess heat.

Synthesis of the Complexes. [(PNEt)$_2$Ir]Y [Y = BPh$_4$ (1a$^+$), PF$_6$ (1b$^+$), Cl (1c$^+$)]. To a solution of PNEt (0.32 g, 1 mmol) in acetone (10 mL) at room temperature was added solid $[Ir(COE)_2Cl]_2$ (0.22 g, 0.25 mmol) to give a red-brown solution. Solid $NaBPh_4$ (0.17 g, 0.5 mmol) was then added with stirring. After 20 min, NaCl was filtered off. On addition of *n*-butyl alcohol (10 mL) and slow evaporation of the solvent under a stream of nitrogen, brown crystals of **1a**$^+$ precipitated in 83% yield. Anal. Calcd for $C_{66}H_{60}N_2BIrP_2$: C, 69.17; H, 5.24; N, 2.44; Ir, 16.79; P, 5.42. Found: C, 69.19; H, 5.28; N, 2.37; Ir, 16.51; P, 5.74. The PF_6^- salt **1b**$^+$ was similarly obtained in 91% yield by using $TlPF_6$ (0.18 g, 0.50 mmol) instead of $NaBPh_4$. Anal. Calcd for $C_{42}H_{40}N_2F_6IrP_3$: C, 51.90; H, 4.12; N, 2.88; Ir, 19.79; P, 9.58. Found: C, 51.70; H, 4.00; N, 3.03; Ir, 19.31; P, 9.47. The chloride salt **1c**$^+$ was obtained in 82% yield by simply adding *n*-butyl alcohol. Anal. Calcd for $C_{42}H_{40}N_2ClIrP_2$: C, 58.49; H, 4.64; N, 3.25; Ir, 22.30; P, 7.20. Found: C, 58.55; H, 4.82; N, 3.33; Ir, 22.10; P, 7.31.

[(PNPr^i)$_2$Ir]Y [Y = BPh$_4$ (2a$^+$), PF$_6$ (2b+), Cl (2c$^+$)]. These compounds were prepared as described above by substituting PNP^i for PNEt. Anal. Calcd for $C_{68}H_{64}N_2BIrP_2$ (**2a**$^+$): C, 69.56; H, 5.46; N, 2.39; Ir, 16.38; P, 5.29. Found: C, 69.55; H, 5.34; N, 2.44; Ir, 16.25; P, 5.31. Anal. Calcd for $C_{44}H_{44}N_2F_6IrP_3$ (**2b**$^+$): C, 52.84; H, 4.40; N, 2.80; Ir, 19.24; P, 9.31. Found: C, 52.77; H, 4.46; N, 2.82; Ir, 19.08; P, 9.28. Anal. Calcd for $C_{44}H_{44}N_2ClIrP_2$ (**2c**$^+$): C, 59.35; H, 4.95; N, 3.15; Ir, 21.60; P, 6.97. Found: C, 59.44; H, 5.00; N, 3.13; Ir, 21.53; P, 6.80.

[(PNBu^t)$_2$Ir]Y [Y = BPh$_4$ (3a$^+$), PF$_6$ (3b$^+$), Cl (3c$^+$)]. These compounds were prepared as described above for **1a**$^+$–**c**$^+$ by substituting PNBu^t for PNEt. Anal. Calcd for $C_{70}H_{68}N_2BIrP_2$ (**3a**$^+$): C, 69.94; H, 5.66; N, 2.33; Ir, 16.00; P, 5.16. Found: C, 69.88; H, 5.60; N, 2.40; Ir, 16.06; P, 5.03. Anal. Calcd for $C_{46}H_{48}N_2F_6IrP_3$ (**3b**$^+$): C, 53.74; H, 4.67; N, 2.73; Ir, 18.71; P, 9.05. Found: C, 53.70; H, 4.50; N, 2.55; Ir, 18.73; P, 9.87. Anal. Calcd for $C_{46}H_{48}N_2ClIrP_2$ (**3c**$^+$): C, 60.15; H, 5.23; N, 3.05; Ir, 20.94; P, 6.76. Found: C, 60.20; H, 5.33; N, 3.03; Ir, 20.87; P, 6.54.

[(PNEt)$_2$Ir(O$_2$)]Y [Y = BPh$_4$ (7a$^+$), PF$_6$ (7b$^+$)]. Compound **1a**$^+$ (0.20 mg, 0.18 mmol) was dissolved in acetone (7 mL). Dioxygen was then bubbled until the color of the solution changed from red-brown to orange (*ca.* 1 min). Addition of *n*-butyl alcohol (10 mL) and slow evaporation

(6) (a) Bianchini, C.; Masi, D.; Meli, A.; Peruzzini, M.; Vacca, A.; Laschi, F.; Zanello, P. *Organometallics* **1991**, *10*, 636. (b) Zanello, P.; Bartocci, C.; Maldotti, A.; Traverso, O. *Polyhedron* **1983**, *2*, 791.

Table 1. Crystallographic Data for $[(PNEt)_2Ir(O_2)]PF_6$

formula	$C_{42}H_{40}N_2F_6IrO_2P_3$
mol wt	1003.91
space group	$P2_1/a$
a (Å)	17.426(4)
b (Å)	14.685(3)
c (Å)	16.131(4)
α (deg)	90.00(0)
β (deg)	98.07(2)
γ (deg)	90.00(0)
V (Å^3)	4087.06
Z	4
D_{calc} (g cm^{-3})	1.63
μ(Cu Kα) (cm^{-1})	79.02
radiation	graphite-monochromated Cu Kα
λ (Å)	1.541 80
R	0.053
R_w	0.056

of the solvent under a stream of nitrogen gave red-orange crystals of **7a**$^+$ in a 80% yield. Anal. Calcd for $C_{66}H_{60}N_2BIrO_2P_2$: C, 67.28; H, 5.10; N, 2.38; Ir, 16.33; P, 5.27. Found: C, 67.22; H, 4.98; N, 2.41; Ir, 16.22; P, 5.22. Compound **7b**$^+$ was prepared in the same manner by using **1b**$^+$ instead of **1a**$^+$. Anal. Calcd for $C_{42}H_{40}N_2F_6IrO_2P_3$: C, 50.24; H, 3.99; N, 2.79; Ir, 19.16; P, 9.27. Found: C, 50.32; H, 4.02; N, 2.82; Ir, 19.24; P, 9.18.

[(PNPr^i)$_2$Ir(O$_2$)]Y [Y = BPh$_4$ (8a$^+$), PF$_6$ (8b$^+$)]. These compounds were prepared as described above using the corresponding deoxygenated complexes. Anal. Calcd for $C_{68}H_{64}N_2BIrO_2P_2$ (**8a**$^+$): C, 67.72; H, 5.31; N, 2.32; Ir, 15.95; P, 5.14. Found: C, 67.54; H, 5.30; N, 2.34; Ir, 15.88; P, 5.17. Anal. Calcd for $C_{44}H_{44}N_2F_6IrO_2P_3$ (**8b**$^+$): C, 52.11; H, 4.34; N, 2.76; Ir, 18.97; P, 9.18. Found: C, 52.09; H, 4.30; N, 2.84; Ir, 18.90; P, 9.24.

[(PNEt)$_2$Ir(CO)]Y [Y = BPh$_4$ (9a$^+$), PF$_6$ (9b$^+$)]. Compound **1a**$^+$ (0.20 mg, 0.18 mmol) was dissolved in acetone (7 mL). Carbon monoxide was then bubbled throughout the red-brown solution. The color of the solution immediately turned orange. Addition of *n*-butyl alcohol (10 mL) and slow evaporation of the solvent under a stream of CO gave orange crystals of **9a**$^+$ in a 89% yield. Anal. Calcd for $C_{67}H_{60}N_2BIrOP_2$: C, 68.54; H, 5.15; N, 2.38; Ir, 16.37; P, 5.28. Found: C, 68.66; H, 5.18; N, 2.44; Ir, 16.09; P, 5.41. Compound **9b**$^+$ was prepared in the same manner by using **1b**$^+$ instead of **1a**$^+$. Anal. Calcd for $C_{43}H_{40}N_2F_6IrOP_3$: C, 51.65; H, 4.03; N, 2.80; Ir, 19.22; P, 9.30. Found: C, 51.58; H, 4.02; N, 2.77; Ir, 19.38; P, 9.22.

X-ray Data Collection and Processing. Crystal and intensity data for **7b**$^+$ are reported in Table 1. X-ray measurements were performed on a Philips PW 1100 diffractometer. The cell constants and orientation matrix were determined by least-squares refinement of the setting angles for 25 reflections. The intensities of three standard reflections were measured every 120 min of X-ray exposure (Cu Kα). An overall decay of ca. 2% was observed. Due to this behavior, the data were corrected on the basis of these standards. The data were also corrected for Lorentz and polarization effects. An empirical correction for the absorption effect was made by using the program DIFABS.[7]

Solution and Refinement of the Structure. All the calculations were carried out on a SEL 32/77 computer, by using the SHELX76[8] and ORTEP[9] programs. Atomic scattering factors were taken from ref 10 for non-hydrogen atoms and from ref 11 for hydrogen atoms. Anomalous dispersion terms, both real and imaginary, were included for non-hydrogen atoms.[12] The function $\sum w(F_o - F_c)^2$ was minimized during the least-squares refinements, the weight w being defined as $1/\sigma^2(F_o)$. The structure was solved by the heavy-atom method. Full-matrix least-squares refinements were carried out by assigning anisotropic thermal parameters to iridium, phosphorus, nitrogen, and oxygen atoms and by treating the phenyl rings as rigid bodies of D_{6h} symmetry. Hydrogen atoms were introduced in their calculated positions (C–H 1.08 Å) and not refined.

(7) Walker, N.; Stuart, D. *Acta Crystallogr.* **1983**, *A39*, 158.
(8) Sheldrick, G. M. SHELX 76: System of Computing Programs. University of Cambridge, Cambridge, England, 1976.
(9) Johnson, C. K. ORTEP. Report ORNL-5138; Oak Ridge National Laboratory: Oak Ridge, TN, 1976.
(10) *International Tables for X-ray Crystallography*; Kynoch Press: Birmingham, England, 1974; Vol. 4, p 99.
(11) Stewart, R. F.; Davidson, E. R.; Simpson, W. T. *J. Chem. Phys.* **1965**, *42*, 3175.
(12) *International Tables for X-ray Crystallography*; Kynoch Press: Birmingham, England, 1974; Vol. 4, p 149.

Table 2. Atomic Parameters for the Structure of $[(PNEt)_2Ir(O_2)]PF_6$[a]

atom	x	y	z	U or U_{eq} (Å^2)
Ir	872(1)	2341(1)	2772(1)	36(1)[b]
P1	591(2)	1514(2)	1597(2)	36(1)
P2	−9(1)	3515(2)	2540(2)	38(1)
P3	1287(3)	1837(3)	6683(2)	80(3)
O1	1908(4)	2675(5)	2447(5)	59(4)
O2	1945(4)	1796(5)	2881(5)	61(5)
N1	126(5)	1477(6)	3309(5)	47(5)
N2	1242(5)	3061(6)	3934(5)	46(5)
C1	362(7)	1187(8)	4194(8)	62(3)
C2	980(10)	482(12)	4205(11)	103(5)
C3	−489(7)	1052(7)	2965(7)	51(3)
C4	−428(6)	1270(6)	1393(6)	41(2)
C5	−832(7)	1220(8)	583(7)	54(3)
C6	−1615(7)	955(8)	443(8)	62(3)
C7	−1997(8)	752(9)	1091(8)	66(3)
C8	−1607(7)	799(8)	1925(8)	61(3)
C9	−829(6)	1067(7)	2074(6)	44(2)
C10	2081(7)	3001(9)	4302(8)	69(3)
C11a	2450(17)	3939(15)	4373(21)	84(8)[c]
C11b	2412(19)	3734(19)	4901(19)	95(10)[c]
C12	814(7)	3468(7)	4405(7)	53(3)
C13	−504(6)	3663(7)	3460(6)	46(2)
C14	−33(7)	3611(7)	4254(7)	51(3)
C15	−383(8)	3780(9)	4983(8)	67(3)
C16	−1156(9)	3979(10)	4933(9)	81(4)
C17	−1611(8)	4036(10)	4160(9)	77(4)
C18	−1271(7)	3886(8)	3425(8)	62(3)
C1,1	1042(3)	391(5)	1698(5)	42(2)
C2,1	619(3)	−395(5)	1811(5)	58(3)
C3,1	999(3)	−1229(5)	1948(5)	87(4)
C4,1	1802(3)	−1277(5)	1973(5)	85(4)
C5,1	2224(3)	−490(5)	1861(5)	60(3)
C6,1	1844(3)	344(5)	1724(5)	50(3)
C1,2	880(4)	1957(4)	642(4)	45(2)
C2,2	1017(4)	2888(4)	570(4)	52(3)
C3,2	1210(4)	3240(4)	−177(4)	64(3)
C4,2	1266(4)	2662(4)	−852(4)	64(3)
C5,2	1128(4)	1731(4)	−780(4)	64(3)
C6,2	936(4)	1379(4)	−33(4)	52(3)
C1,3	464(3)	4619(5)	2521(5)	45(2)
C2,3	45(3)	5415(5)	2603(5)	66(3)
C3,3	410(3)	6260(5)	2603(5)	82(4)
C4,3	1195(3)	6309(5)	2620(5)	89(4)
C5,3	1615(3)	5513(5)	2438(5)	84(4)
C6,3	1249(3)	4668(5)	2438(5)	59(3)
C1,4	−746(4)	3581(5)	1606(5)	47(2)
C2,4	−550(4)	4053(5)	915(5)	62(3)
C3,4	−1054(4)	4052(5)	162(5)	75(4)
C4,4	−1754(4)	3579(5)	101(5)	75(4)
C5,4	−1950(4)	3108(5)	792(5)	67(3)
C6,4	−1446(4)	3108(5)	1544(5)	50(3)
F1	1911(7)	1755(9)	7484(8)	146(4)
F2	1294(9)	2899(11)	6971(10)	177(5)
F3	632(7)	1705(8)	7218(8)	139(4)
F4	719(9)	2139(11)	5919(10)	179(5)
F5	1990(10)	2018(12)	6191(11)	209(7)
F6	1378(9)	878(11)	6460(10)	186(6)

[a] Thermal parameters multiplied by 10^3; coordinates, by 10^4. [b] U_{eq} defined as one-third of the trace of the orthogonalized thermal tensor. [c] Atoms C11a and C11b were assigned an occupancy factor of 0.5.

The refinement converged to $R = 0.053$ and $R_w = 0.056$ factors. The ΔF final maps appeared essentially featureless. Final positional parameters for non-hydrogen atoms of **7b**$^+$ are reported in Table 2.

Results

Synthesis and Characterization of the Iridium(I) Complexes. Brown crystals of $[(PNalkyl)_2Ir]Cl$ (**1c**$^+$–**3c**$^+$) are obtained in excellent yield by treatment of $[Ir(COE)_2Cl]_2$ in acetone with a 2-fold excess of the appropriate PNalkyl ligand. Metathetical reactions with either $NaBPh_4$ or $TlPF_6$ give the corresponding tetraphenylborate (**1a**$^+$–**3a**$^+$) or hexafluorophosphate (**1b**$^+$–**3b**$^+$) derivatives. Irrespective of the counterion, all the Ir(I) complexes **1**$^+$–**3**$^+$ are isolated as crystals which are stable under a nitrogen

Table 3. ^{31}P NMR and ^1H NMR Spectral Data for the Complexes[a]

complex	^{31}P NMR	^1H NMR
$[(PNEt)_2Ir]^+$	A_2 spin system; $\delta(P)$ 23.45	$\delta(CH_3)$ 1.52 (6H, t) $\delta(CH_2)$ 4.06 (4H, q); $J(HH)$ 7.3 Hz $\delta(N{=}CH)$ 8.76 (2H, d); $J(HP)$ 7.2 Hz
$[(PNEt)_2Ir(O_2)]^+$	AB spin system; $\delta(P_A)$ −6.49, $\delta(P_B)$ −7.90; $J(PP)$ 12.2 Hz	$\delta(CH_3)$ 1.26 (3H, t); $J(CH_3H)$ 7.2 Hz $\delta(CH_A)$ 3.97 (1H, dqd); $J(H_AP)$ 3.0, $J(H_AH_B)$ 12.1, $J(H_ACH_3)$ 7.5 Hz $\delta(CH_B)$ 3.74 (1H, dqd); $J(H_BP)$ 3.0, $J(H_AH_B)$ 12.1, $J(H_BCH_3)$ 7.0 Hz $\delta(N{=}CH)$ 8.77 (1H, d); $J(HP)$ 11.3 Hz $\delta(CH_3')$ 1.11 (3H, t); $J(CH_3'H')$ 7.2 Hz $\delta(CH_A')$ 4.37 (1H, dqd); $J(H_A'P)$ 2.0, $J(H_A'H_B')$ 11.6, $J(H_A'CH_3')$ 6.9 Hz $\delta(CH_B')$ 3.58 (1H, dqd); $J(H_B'P)$ 1.7, $J(H_A'H_B')$ 11.6, $J(H_B'CH_3')$ 7.5 Hz $\delta(N{=}CH')$ 8.77 (1H, s)
$[(PNEt)_2Ir(CO)]^+$ [b]	A_2 spin system; $\delta(P)$ 29.39	$\delta(CH_3)$ 0.63 (6H, t) $\delta(CH_2)$ 2.99 (4H, q); $J(HH)$ 7.2 Hz $\delta(N{=}CH)$ 8.38 (2H, s)
$[(PNPr^i)_2Ir]^+$	A_2 spin system; $\delta(P)$ 22.16	$\delta(CHCH_3CH_3)$ 1.52 (6H, d); $J(HH)$ 6.6 Hz $\delta(CHCH_3CH_3)$ 1.50 (6H, d); $J(HH)$ 6.6 Hz $\delta(CH)$ 4.27 (2H, sept); $J(HH)$ 6.6 Hz $\delta(N{=}CH)$ 8.74 (2H, d); $J(HP)$ 7.5 Hz
$[(PNPr^i)_2Ir(O_2)]^+$	AB spin system; $\delta(P_A)$ −5.65, $\delta(P_B)$ −6.33; $J(PP)$ 12.9 Hz	$\delta(CH_{3A}')$ 0.97 (3H, d); $J(CH_{3A}'H')$ 6.6 Hz $\delta(CH_{3B}')$ 1.23 (3H, d); $J(CH_{3B}'H')$ 6.5 Hz $\delta(CH')$ 4.39 (1H, sept); $J(HCH_3')$ 6.6 Hz $\delta(N{=}CH')$ 8.94 (1H, s) $\delta(CH_{3A})$ 0.81 (3H, d); $J(CH_{3A}H)$ 6.8 Hz $\delta(CH_{3B})$ 1.38 (3H, d); $J(CH_{3B}H)$ 6.6 Hz $\delta(CH)$ 5.11 (1H, sept of d); $J(HCH_3)$ 6.7, $J(HP)$ 1.6 Hz $\delta(N{=}CH)$ 8.81 (1H, d); $J(HP)$ 10.6 Hz
$[(PNBu^t)_2Ir]^+$	A_2 spin system; $\delta(P)$ 22.47	$\delta(C(CH_3)_3)$ 1.46 (18H, s) $\delta(N{=}CH')$ 8.80 (2H, d); $J(HP)$ 5.8 Hz

[a] All spectra were recorded at room temperature (296 K) in CD_3COCD_3 unless otherwise stated. [b] In CO-saturated solution.

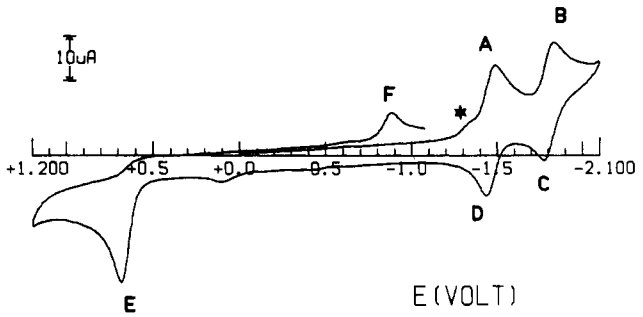

Figure 1. Cyclic voltammogram recorded at a platinum electrode on a deareated Me_2CO solution containing **1b**$^+$ (1.50×10^{-3} M) and $(NBu_4)ClO_4$ (0.2 M). Scan rate: 0.2 V s^{-1}. T = 20 °C.

atmosphere in both the solid state and solution. The IR spectra show bands in the 1600–1630-cm^{-1} region readily assigned to $\nu(C{=}N)$ vibrations of the imino group.[4] All compounds are moderately soluble in common organic solvents in which they behave as 1:1 electrolytes. For all compounds, the ^1H and ^{31}P NMR spectra (CD_3COCD_3, 296 K) show that the two ligands coordinated to iridium are magnetically equivalent in the temperature range from −70 to +30 °C (Table 3). Indeed, the ^{31}P NMR spectra invariably consist of singlets with chemical shifts in the typical range of Ir(I) complexes. Likewise, the ^1H NMR spectra show single sets of resonances for the nonequivalent protons of the alkyl substituents. Appreciable coupling (J = 5–7 Hz) to the phosphorus atom is exhibited by the C*H*=N protons, which indicates that the CH=N groups are *trans* to the phosphorus atoms. Thus, the spectroscopic data are consistent with a square-planar coordination geometry in which the phosphorus atoms are *cis* to each other, as previously reported for the Rh congeners $[(PNalkyl)_2Rh]^+$.[4]

Electrochemistry of the Iridium(I) Complexes. Figure 1 shows the cyclic voltammetric response exhibited by **1b**$^+$ in acetone solution. The complex cation undergoes two distinct reduction processes (at peaks A and B, respectively) as well as one oxidation process (at peak E). As shown by the appearance of the directly associated peaks C and D, the two reduction steps display features of chemical reversibility. In contrast, the anodic process appears in the reverse scan, as peak F, which is located far away from the position expected for a directly associated response, thus indicating irreversible decomposition of the oxidation product. Finally, the minor feature labeled by an asterisk indicates the presence of a very low amount of oxygenated product **7b**$^+$ (see below).

At room temperature, controlled-potential coulometry corresponding to the first cathodic step A (E_w = −1.6 V) shows that the current abrupty falls after the consumption of 1 electron/molecule but remains higher than the background current up to an overall consumption of about 4 electrons/molecule. The resulting solution no more exhibits well-defined redox curves in cyclic voltammetry. In contrast, controlled-potential coulometry performed at −15 °C shows a net consumption of 1 electron/molecule; the resulting solution exhibits a cyclic voltammetric profile quite complementary to the one shown in Figure 1. These data indicate that, at room temperature, the electrogeneration of the uncharged species $[(PNEt)_2Ir]$ (**1b**) is complicated by slow decomposition to further electroreducible products whereas at low temperature the decomposition is fully prevented.

Analysis[13] of the cyclic voltammetric responses relevant to the peak system A/D with scan rate v varying from 0.02 to 20.48 V s^{-1} shows that (i) the anodic-to-cathodic current ratio i_{pD}/i_{pA} is constantly equal to 1; (ii) the current function $i_{pA}\,v^{-1/2}$ remains substantially constant, and (iii) the peak-to-peak separation $\Delta E_p = E_{pD} - E_{pA}$ is equal to 60 mV at the lowest scan rates (up to 0.2 V s^{-1}), and then it slightly tends to increase to 130 mV at the highest scan rate, probably because of the presence of some uncompensated solution resistances. These data are diagnostic of an electrochemically reversible 1-electron addition and, therefore, are consistent with no important structural changes accompanying the Ir^I/Ir^0 (see below) redox process **1b**$^+$/**1b**.[14,15]

The second cathodic step, which on the cyclic voltammetry time scale apparently involves a 1-electron addition, is complicated

(13) Brown, E. R.; Sandifer, J. R. In *Physical Methods of Chemistry. Electrochemical Methods*; Rossiter, B. W., Hamilton, J. F., Eds.; Wiley: New York, 1986; Vol. 2, Chapter IV.

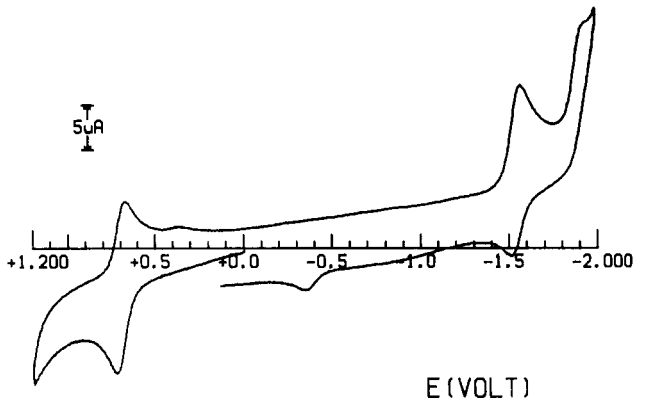

Figure 2. Cyclic voltammogram recorded at a platinum electrode on a deareated Me_2CO solution containing $\mathbf{3b}^+$ (1.20×10^{-3} M) and $(NBu_4)ClO_4$ (0.2 M). Scan rate: 0.2 V s^{-1}. T = 20 °C.

by fast decomposition of the instantaneously electrogenerated monoanion $[(PNEt)_2Ir]^-$ ($\mathbf{1b}^-$). The reoxidation peak C, which is practically absent at scan rates lower than 0.1 V s^{-1}, becomes visible at higher scan rates (the i_{pC}/i_{pB} ratio reaches the value of 1 at about 1 V s^{-1}). A lifetime ($t_{1/2}$) of about 1 s can roughly be computed for $\mathbf{1b}^-$ at ambient temperature.[13]

Finally, the anodic process occurring at peak E, which in cyclic voltammetry seems to involve a 2-electron removal, shows no directly associated response in the reverse scan even at 20.48 V s^{-1}. Because of such irreversible degradation, no further study was devoted to it.

Complex $\mathbf{2b}^+$ displays a redox behavior qualitatively similar to that of $\mathbf{1b}^+$. In contrast, as illustrated in Figure 2, the cation $\mathbf{3b}^+$ exhibits a significantly different redox behavior in the anodic region. In fact, it shows a reversible Ir^I/Ir^{II} step, though complicated by slow decomposition, in which the cathodic-to-anodic peak current ratio is 0.50 at 0.02 V s^{-1} but quickly reaches a value of unity at 0.5 V s^{-1}.

Controlled-potential coulometry at −15 °C shows the occurrence of a stepwisel $Ir^I/Ir^{II}/Ir^{III}$ electrode process. As shown in Figure 3a, after the consumption of 0.7 electron/molecule, $\mathbf{3b}^+$ is almost completely oxidized to $[(PNBu^t)_2Ir]^{2+}$ ($\mathbf{3b}^{2+}$) ($E^{\circ\prime}_{2+/+}$ = +0.58 V *vs* Ag/AgCl), but another compound appears, which undergoes reduction a E_p = +0.22 V. Then the electrolysis current abruptly falls but remains higher than the residual current. As illustrated in Figure 3b, after the overall consumption of 1.7 electrons/molecule, the second Ir(II) product becomes the predominant one. The current decays after the consumption of 2 electrons/molecule. All these data provide evidence of the occurrence of the following ECE mechanism, which is also supported by the ESR experiments reported in the next section:

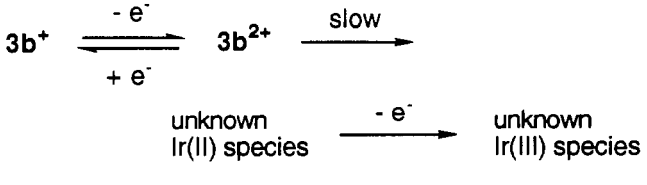

The redox potentials for the electron-transfer processes exhibited by all the complexes are summarized in Table 4.

Substitution of CH_2Cl_2 for acetone in the electrochemical experiments does not change the electron-transfer picture for all complexes, indicating that the potential coordinating ability of acetone does not apparently play a role in the stabilization or degradation of the electrochemically generated products.

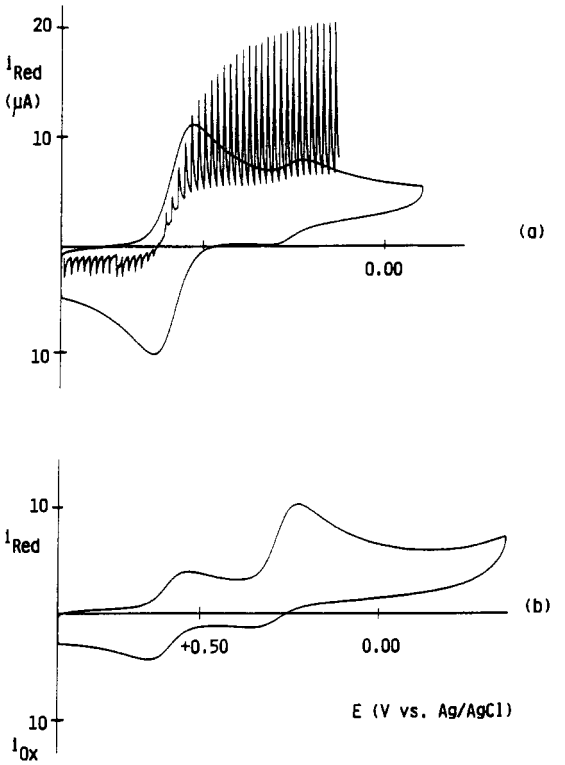

Figure 3. Cyclic and dc voltammograms recorded at a platinum electrode, after macroelectrolysis tests (E_w = +0.7 V)at −15 °C on a deareated Me_2CO solution containing $\mathbf{3b}^+$ (1.50×10^{-3} M) and $(NBu_4)ClO_4$ (0.2 M): (a) after consumption of 0.7 electron/molecule; (b) after consumption of 1.7 electrons/molecule. T = −15 °C. Scan rates: CV, 0.2 V s^{-1}; DCV, 0.02 V s^{-1}.

Electron Spin Resonance of the Paramagnetic Iridium(0) and Iridium(II) Congeners. Figure 4 shows the frozen-solution (100 K) X-band ESR spectrum of the neutral species **1b** electrogenerated in acetone solution at −15 °C. The signal exhibits a well-resolved axial structure ($g_\parallel > g_\perp$) attributable to a $S = {}^1/_2$ paramagnetic species having a metal-centered unpaired electron: $g_\parallel$ = 2.035 ± 0.005; $g_\perp$ = 1.999 ± 0.005; $\langle g \rangle = (g_\parallel + 2g_\perp)/3$ = 2.011 ± 0.005.

The second-derivative line shape analysis allows one to detect in the perpendicular region a poorly resolved 1:2:1 triplet, likely arising from the interaction of the unpaired electron with the two ^{31}P nuclei ($I = {}^1/_2$) of the ligands ($a_\perp$ = 10 ± 5 G). No appreciable coupling of the unpaired electron to the ^{193}Ir nucleus is observed, which is consistent with several literature data.[16]

The ESR analysis is supported by a computer simulation of the experimental spectrum (SIM 14A program).[17] At 195 K the ESR signal becomes isotropic with g_{iso} and ΔH_{iso} values of 2.008 ± 0.005 and 30 ± 5 G, respectively, which fit the corresponding calculated parameters.

Figure 5 shows the ESR spectrum recorded at 100 K on a Me_2CO sample withdrawn at the first stages of the anodic electrolysis of $\mathbf{3b}^+$ at −15 °C. The rather complex line shape displays four distinct absorptions. On the basis of both second-derivative analysis and computer simulation, the glassy spectrum can be interpreted in terms of two sets of signals arising from the presence of two paramagnetic ($S = {}^1/_2$) species **A** and **B** in a *ca.* 4:1 ratio. The relevant parameters of the two species are as follows. A: $g_\parallel$ = 2.240 ± 0.005; $g_\perp$ = 1.959 ± 0.005; $\langle g \rangle = (g_\parallel + 2g_\perp)/3$

(14) Zanello, P. In *Stereochemistry of Organometallic and Inorganic Compounds*; Bernal, I., Ed.; Elsevier: Amsterdam, 1990; Vol. 4, p 181.
(15) Zanello, P. *Struct. Bonding (Berlin)* **1992**, *79*, 101.
(16) (a) Barbaro, P.; Bianchini, C.; Linn, K.; Mealli, C.; Meli, A.; Laschi, F.; Zanello, P. *Inorg. Chim. Acta* **1992**, *200*, 31. (b) García, M. P.; Jiménez, M. V.; Oro, L. A.; Lahoz, F. J.; Alonso, P. j. *Angew. Chem., Int. Ed. Engl.* **1992**, *31*, 1527. (c) Mason, R.; Thomas, K. M.; Empsall, H. D.; Fletcher, S. R.; Heys, P. N.; Hyde, E. M.; Jones, C. E.; Shaw, B. L. *J. Chem. Soc., Chem. Commun.* **1974**, 612.
(17) Lozos, J. P.; Hoffman, B. M.; Franz, C. G. QCPE Program No 265. Chemistry Department, Northwestern University, Evanston, IL, 1974.

Table 4. Formal Electrode Potentials for the Electron-Transfer Processes Exhibited by the Complexes $[(PNalkyl)_2Ir]PF_6$ ($1b^+$–$3b^+$) and $[(PNalkyl)_2Rh]PF_6$ ($4b^+$–$6b^+$) in Acetone Solution

		reduction processes				oxidation processes		
complex	R	$E°'_{+/0}$ (V)	$\Delta E_p{}^a$ (mV)	$E°'_{0/-}$ (V)	$\Delta E_p{}^a$ (mV)	$E°'_{2+/+}$ (V)	$\Delta E_p{}^a$ (mV)	$E_{p,3+/+}{}^{a,b}$ (V)
1b$^+$	Et	−1.45	62	−1.79	72			+0.63
2b$^+$	Pr^i	−1.50	65	−1.90[a,b]				+0.70
3b$^+$	Bu^t	−1.51	80	−1.92[a,b]		+0.71	68	
4b$^+$	Et	−1.52	100	−1.89[a,b]				+0.72
		−1.52[c]	86[c]	−1.81[c]	126[c]			+0.75[c]
5b$^+$	Pr^i	−1.56	78	−1.89[a,b]				+0.69
		−1.56[c]	78[c]	−1.84[c]	114[c]			+0.70[c]
6b$^+$	Bu^t	−1.60	92	−1.92[a,b]		*d*		
		−1.58[c]	62[c]	−1.89[c]	80[c]	+0.76[c]	59[c]	

[a] Measured at 0.2 V s^{-1}. [b] Forward peak potential. [c] Measured at −20 °C. [d] Difficult to evaluate because of chemical complications.

Figure 4. X-Band ESR spectrum of a Me_2CO solution of **1b** recorded at 100 K.

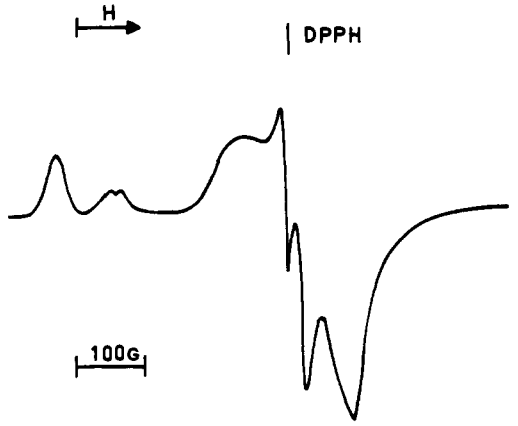

Figure 5. X-Band ESR spectrum of a Me_2CO solution of **3b**$^+$ withdrawn after the consumption of 0.7 electron/molecule in anodic electrolysis, recorded at 100 K.

= 2.053 ± 0.005; $\Delta H_\parallel$ = 40 ± 5 G; $\Delta H_\perp$ = 80 ± 5 G. **B**: $g_\parallel$ = 2.166 ± 0.005; $g_\perp$ = 1.999 ± 0.005; $\langle g \rangle = (g_\parallel + 2g_\perp)/3$ = 2.055 ± 0.005. Both absorption patterns are characteristic of metal-centered systems. On the basis of the electrochemical results, the most abundant species is confidently recognized as the Ir(II) dication **3b**$^{2+}$. The second iridium(II) species **B**, which is most likely responsible for the further 1-electron oxidation process, shows hyperfine splitting (1:1 pattern) in both the perpendicular and parallel regions, thus indicating appreciable interaction of the unpaired electron with one ^{31}P nucleus only ($A_\parallel$ = 40 ± 5 G; $A_\perp$ = 80 ± 5 G).

Electrochemistry of the Rhodium(I) Complexes 4b$^+$–6b$^+$. As previously mentioned, the mixed-donor PNalkyl ligands are capable of forming Rh(I) complexes which are isostructural with the iridium ones.[4]

The electrochemical behavior of the Rh(I) complexes is qualitatively similar to that of the iridium(I) analogues. The

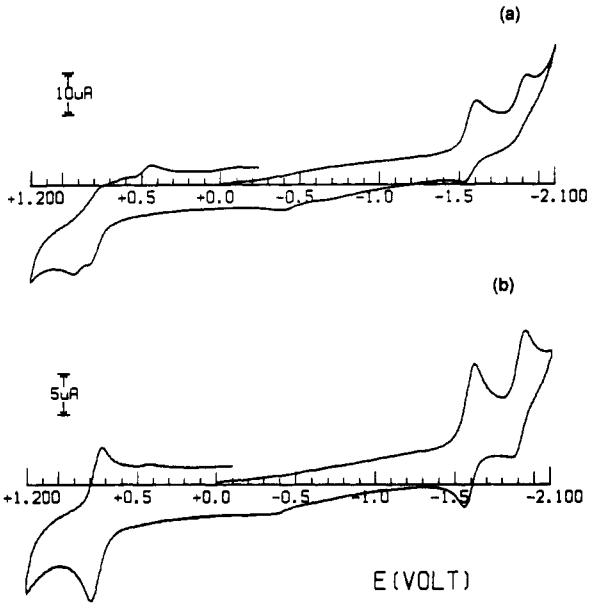

Figure 6. Cyclic voltammograms recorded at a platinum electrode on a deareated Me_2CO solution containing **6b**$^+$ (8.0×10^{-4} M) and $(NBu_4)ClO_4$ (0.2 M): (a) T = 20 °C; (b) T = −20 °C. Scan rate: 0.2 Vs^{-1}.

Rh(II) and Rh(0) redox congeners, however, are less stable than the corresponding iridium complexes. This is illustrated in Figure 6, which shows that all the redox processes of **6b**$^+$ are complicated by subsequent decomposition processes at ambient temperature, whereas at −20 °C features of significant chemical reversibility are clearly visible.

The electrode potentials for the redox changes exhibited by complexes **4b**$^+$–**6b**$^+$ are compared with those of complexes **1b**$^+$–**3b**$^+$ in Table 4. It is worth noticing that, in spite of the higher atomic number of iridium, the reduction of the iridium complexes is slightly easier than that of the rhodium congeners.

Electron Spin Resonance of the Paramagnetic Rhodium(0) and Rhodium(II) Congeners. As for the iridium(0) analogue **1b**, the liquid nitrogen ESR parameters of the electrogenerated rhodium(0) species $[(PNEt)_2Rh]$ (**4b**) are consistent with an axial symmetry. The relevant parameters are as follows: $g_\parallel$ = 2.094 ± 0.005; $g_\perp$ = 2.010 ± 0.005; $\langle g \rangle = (g_\parallel + 2g_\perp)/3$ = 2.038 ± 0.005. At the glassy–fluid transition (T = 178 K), the spectral signal becomes isotropic with g_{iso} = 2.037 ± 0.005 (ΔH_{iso} = 25 ± 5 G).

The second-derivative analysis, carried out on both glassy and fluid solutions, does not allow one to identify any hyperfine resolution of the absorption signals, likely as a result of active line-broadening effects.

The ESR spectrum recorded on solutions of **6b**$^+$ withdrawn at the first stages of the anodic electrolysis (E_w = +1.0 V) at −15 °C displays a very complex pattern arising from the presence of more than two paramagnetic species whose signals overlap. As

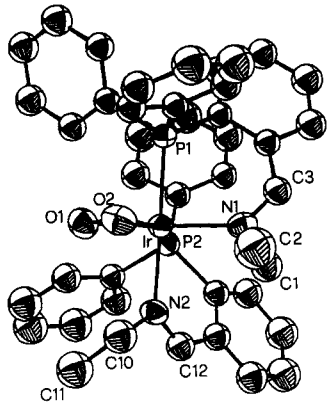

Figure 7. ORTEP drawing of the complex cation $[(PNEt)_2Ir(O_2)]^+$ showing the labeling scheme.

Table 5. Selected Bond Distances (Å) and Angles (deg) for $[(NPEt)_2Ir(O_2)]PF_6$

Ir–P1	2.255(2)	Ir–N1	2.099(9)
Ir–P2	2.292(2)	Ir–N2	2.162(8)
Ir–O1	2.007(8)	O1–O2	1.47(1)
Ir–O2	2.025(8)		
N1–Ir–N2	93.7(3)	N2–Ir–P1	174.0(2)
N1–Ir–O2	109.6(3)	O2–Ir–O1	42.6(3)
N1–Ir–O1	152.2(3)	O2–Ir–P2	154.6(2)
N1–Ir–P2	94.8(3)	O2–Ir–P1	86.6(2)
N1–Ir–P1	86.6(2)	O1–Ir–P2	112.8(2)
N2–Ir–O2	87.7(3)	O1–Ir–P1	90.4(2)
N2–Ir–O1	86.7(3)	P2–Ir–P1	102.0(1)
N2–Ir–P2	83.9(2)		
	P2–Ir–N2–C12	38.6(9)	
	P1–Ir–N1–C1	139.9(7)	

for iridium, the electrochemical evidence for rhodium shows that the expected ECE oxidation process of **6b**$^+$ is further complicated by fast fragmentation of the intermediate rhodium(II) congener.

Synthesis and Characterization of the Dioxygen Complexes. Compounds **1a**$^+$,**b**$^+$ and **2a**$^+$,**b**$^+$ react rapidly and quantitatively at room temperature with O_2 (1 atm) in acetone solution to give orange complexes of formula $[(PNalkyl)_2Ir(O_2)]Y$ (**7a**$^+$,**b**$^+$ and **8a**$^+$,**b**$^+$). Crystals can be isolated by adding *n*-butyl alcohol to the acetone solutions. All the dioxygen adducts are stable in deoxygenated solutions even at high temperature (DMSO-d_6, 363 K). In contrast, complexes **3a**$^+$–**c**$^+$ do not appreciably react with dioxygen in solution even at low temperature (^{31}P NMR, CD_3COCD_3, 203 K). Complexes **7a**$^+$,**b**$^+$ and **8a**$^+$,**b**$^+$ are moderately soluble in common organic solvents in which they behave as 1:1 electrolytes.

In contrast to $Ir(CO)Cl(PPh_3)_2(O_2)$, whose deoxygenation is principally photochemical as recently shown by Selke and Foote,[18] compounds **7a**$^+$,**b**$^+$ and **8a**$^+$,**b**$^+$ are stable when exposed to sunlight or to a standard tungsten lamp. Only upon irradiation with a UV lamp (principal emission 366 nm) does photolysis of the dioxygen complexes occur. However, this occurs within a few minutes and essentially results in their decomposition (ony traces, 2–3%, of the deoxygenated species are formed). Since the precursors **1a**$^+$,**b**$^+$ and **2a**$^+$,**b**$^+$ are fully stable under analogous experimental conditions, one may reasonably conclude that UV irradiation actually promotes decomposition of the oxygenated species.

An X-ray analysis carried out on **7b**$^+$ shows that the molecular structure consists of complex cations $[(PNEt)_2Ir(O_2)]^+$ and PF_6^- anions. An ORTEP view of the cation is reported in Figure 7, while selected bond distances and angles are reported in Table 5. The coordination geometry around the metal center in the complex cation can be described as either a distorted octahedron or a distorted trigonal bipyramid according to whether the coordinated dioxygen molecule is treated as occupying one or two coordination sites. In the octahedral picture, the distortion from idealized geometry is mainly due to the short separation between the two oxygen atoms [O1–O2 1.47(1) Å], which is typical of peroxo complexes of transition metals.[3a] There is a small axial elongation along the P1–Ir–N2 axis. In the distorted trigonal-bipyramidal geometry, the phosphorus atom (P2) of one PNEt ligand, the nitrogen atom (N1) of the other ligand, and the peroxo group would lie in the equatorial positions. Irrespective of the geometry, the phosphorus and nitrogen atoms of a same ligand are *cis* to each other, while the phosphorus atom of one ligand (P1) is *trans* to the nitrogen atom (N2) of the other ligand. The atoms P2, N1, O1, O2, and Ir lie on the same plane within experimental error. Finally, while the Ir–O bond distances [which are in the typical range for the Ir(η^2-O_2) moiety[3a,b]] appear almost equivalent (2.007(8) and 2.025(8) Å), a small difference in the bonding distances of the two PNEt ligands to the metal is visible [Ir–P1 2.255(2) *versus* Ir–P2 2.292(2) Å and Ir–N1 2.099(9) *versus* Ir–N2 2.162(8) Å]. It is noteworthy that the O–O distance [1.47(1) Å] in **7b**$^+$ is significantly longer than the analogous separation in the Rh derivative $[(PNPr^i)_2Rh(O_2)]$ [1.436(9) Å].[4]

The ^{1}H and ^{31}P NMR spectra (Table 3) of samples in CD_3-$COCD_3$ solution are consistent with the geometry found in the solid state. In fact, the ^{31}P NMR spectrum (296 K) consists of an AB spin system, indicating the chemical nonequivalence of the two phosphorus nuclei. The two phosphorus signals are upfield-shifted with respect to those of the corresponding deoxygenated complex due to the change in the formal oxidation state of iridium from +1 to +3 upon oxidative addition of O_2. The J(PP) coupling constant is consistent with the *cis* position of the two phosphorus atoms.[19] The ^{1}H NMR spectrum shows that the hydrogens of the two ethyl residues and of the two imino groups are magnetically nonequivalent. Each ethyl residue shows a set of resonances characteristic of two diasterotopic methylenic protons (H_A and H_B in Table 3) coupled to each other ($J \sim 12$ Hz) and to the protons of the geminal methyl group ($J \sim 7$ Hz). A small coupling interaction with one phosphorus atom gives rise to a dqd pattern for the resonances of each methylenic proton, while each methyl group appears as a triplet. A perusal of Table 3 shows that the hydrogens of the CH=NEt group belonging to one ligand exhibit larger J(HP) coupling constants than those of the hydrogens of the other ligand (primed in Table 3). The hydrogen atoms exhibiting larger J(HP) values are therefore attributed to the CH=NEt group *trans* to the phosphorus atom. Such an assignment was confirmed by selective homo- and heteronuclear decoupling experiments. Analogous conclusions are valid for the complex cation $[(PNiPr^i)_2Ir(O_2)]^+$ even though the corresponding ^{1}H NMR spectrum is less complex. In this case, the resonances of the CH protons of the Pr^i substituents appear as either a septuplet or a septuplet of doublets depending on the J(HP) values (Table 3).

Electrochemistry of the Dioxygen Adducts. Figure 8 shows the cyclic voltammetric response exhibited by **7b**$^+$ in acetone solution. The complex undergoes a main reduction step at peak A, which displays a well-defined reoxidation response in the reverse scan only at very high scan rates (Figure 8c). Controlled-potential coulometry (E_w = −1.5 V) consumes 1 electron/molecule, thus suggesting that the reduction process **7b**$^+$/**7b** ($E^{\circ\prime}$ = −1.31 V) involves the IR^{III}/Ir^{II} moiety rather than the peroxo fragment (the reduction of which would consume 2 electrons/molecule). A rough evaluation of the lifetime of **7b** gives a value of 0.02 s.

In contrast, the anodic step at E_p = +0.83 V is assigned to the oxidation of the peroxo group. We have not investigated the underlying mechanism of this process, which manifests a degree of reversibility higher than the one illustrated in Figure 1 for the corresponding oxygen-free species.

(18) Selke, M.; Foote, C. S. *J. Am. Chem. Soc.* **1993**, *115*, 1166.

(19) Pregosin, P. S.; Kunz, R. W. In *^{31}P and ^{31}C NMR of Transition Metal Phosphine Complexes*; Diehl, P., Fluck, E., Kosfold, R., Eds.; Springer: Berlin, Heidelberg, 1979.

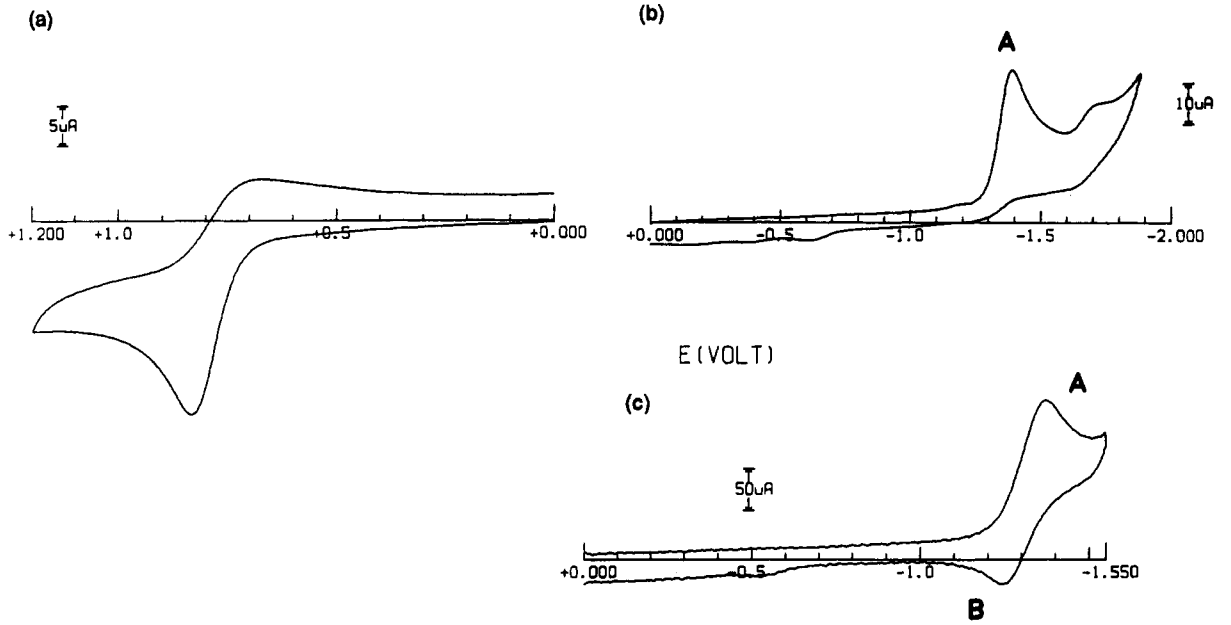

Figure 8. Cyclic voltammetric responses recorded at a platinum electrode on a deareated Me_2CO solution containing $\mathbf{7b}^+$ (1.60×10^{-3} M) and $(NBu_4)ClO_4$ (0.2 M). Scan rates: (a, b) 0.2 V s^{-1}; (c) 10.24 V s^{-1}.

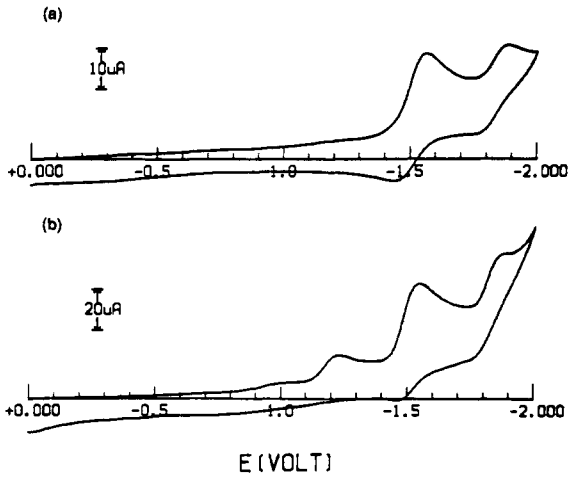

Figure 9. Cyclic voltammetrijc responses recorded at a platinum electrode on (a) a deareated Me_2CO solution containing $\mathbf{4b}^+$ (1.70×10^{-3} M) and $(NBu_4)ClO_4$ (0.2 M) and (b) solution a after O_2 bubbling for 5 min, followed by Ar deareation for 15 min. Scan rate: 0.2 V s^{-1}. $T = 20$ °C.

Compound $\mathbf{8b}^+$ displays similar cyclic voltammetric behavior ($E_p = -1.36$ V).

As for the rhodium complexes, it has previously been reported that they add dioxygen reversibly.[4] Nevertheless, the release of dioxygen under argon bubbling is not immediate. The gradual loss of dioxygen is documented in Figure 9 for $\mathbf{4b}^+$, in which we show the effect of bubbling dioxygen for 5 min, followed by deareation for 15 min.

There is clear evidence for the presence of some oxygenated complex, which undergoes an irreversible reduction at $E_p = -1.23$ V. Such an irreversible peak completely disappears only after bubbling argon for *ca.* 1 h.

The same behavior is observed upon bubbling O_2/Ar through solutions of $\mathbf{5b}^+$, the irreversible reduction peak of the oxygenated species being located at $E_p = -1.28$ V. In the case of $\mathbf{6b}^+$, we were unable to localize the reduction peak of the relevant dioxygen complex, if any.

Synthesis and Characterization of the Carbonyl Complexes. When CO is bubbled at room temperature into acetone solutions of $\mathbf{1a}^+$,$\mathbf{b}^+$, an immediate color change from brown to red-orange occurs. Orange crystals of the CO adducts $\mathbf{9a}^+$,$\mathbf{b}^+$ are obtained by addition of *n*-butyl alcohol under a CO atmosphere. The reactions are quantitative (^{31}P NMR spectroscopy) and are completely reversible at room temperature upon substitution of a nitrogen atmosphere for an oxygen atmosphere. Complexes $\mathbf{9a}^+$,$\mathbf{b}^+$ are moderately soluble in common organic solvents in which they behave as 1:1 electrolytes. The IR spectra contain carbonyl stretching bands [ν(CO) = 1973 cm^{-1}] in the expected range of iridium(I) carbonyls.[20] ^1H and ^{31}P NMR spectra of $\mathbf{9a}^+$,$\mathbf{b}^+$ (Table 3) show the two PNEt ligands to be magnetically equivalent. Accordingly, both compounds are assigned square-pyramidal structures with the carbonyl ligand located in the apical position. Formation of analogous carbonyl complexes is observed for $\mathbf{2a}^+$–$\mathbf{c}^+$, whereas $\mathbf{3a}^+$–$\mathbf{c}^+$ do not react with CO under comparable reaction conditions.

Discussion

Redox Chemistry. In the Ir(I) complexes described in this paper as well as the Rh(I) congeners, any π contribution of the PNalkyl ligands to the description of the MO frontier orbitals may be considered almost negligible, and therefore, one can use the well-known orbital interaction diagram of square-planar ML_4 complexes[21] for a qualitative rationalization of the redox chemistry, the ESR spectra, and the uptake of either O_2 or CO. If so, the HOMO and the LUMO would consist primarily of metal z^2 and x^2-y^2 orbitals, respectively. This is consistent with the ESR spectra of the electrogenerated M(II) and M(0) complexes (M = Rh, Ir), which show that the unpaired electron is essentially localized on the metal center.

The addition and removal of electrons (only for alkyl = Bu^t) are electrochemically reversible, indicating that both electron-transfer processes do not apparently induce a drastic change in the primary geometry of the starting $[(PNalkyl)_2M]^+$ complexes. These have been assigned a square-planar geometry on the basis of NMR spectra. However, some distorsion from idealized geometry is probably present as a consequence of the *cis* disposition of the alkyl-substituted nitrogen donors. Indeed, an X-ray analysis of a related Ir(I) complex of formula $[(PNNP)Ir]^+$ (PNNP = 2,2′-bis[[*o*-(diphenylphosphino)benzylidene]amino]-6,6′-dime-

(20) Leigh, G. J.; Richards, R. L. In *Comprehensive Organometallic Chemistry*; Wilkinson, G., Stone, F. G. A., Abel, E. W., Eds.; Pergamon Press: Oxford, England, 1982; Vol. 5, p 542.

(21) (a) Albright, T. A.; Burdett, J. K.; Whangbo, M. H. *Orbital Interactions in Chemistry*; Wiley–Interscience: New York, 1985. (b) Hoffmann, R.; Chen, M. M. L.; Thorn, D. L. *Inorg. Chem.* **1977**, *16*, 503.

thylbiphenyl) showed that the metal adopts a distorted square-planar structure, the non perfectly planar nature of the coordination geometry being attributed to the twist between the phenyl rings attached to tbe N substituents.[22]

It is worth discussing the fact that, irrespective of the N substituent, all the Ir and Rh complexes are reversibly reduced to the corresponding M(0) derivatives, whereas only for the bulkiest substituent (Bu^t) are the paramagnetic M(II) species stable, even though at low temperature. The most straightforward interpretation of this substituent effect is to think that the Bu^t groups may "chemically" stabilize the Ir(II) and Rh(II) complexes; *i.e.*, the Bu^t groups might "protect" the radical metal center from external attack by either the solvent or traces of dioxygen as it occurs in the parent M(I) derivatives. On the other hand, one cannot exclude that, upon 1-electron oxidation, the starting M(I) complexes may undergo a further distortion of the coordination geometry so as to make the M(II) complexes susceptible to a second fast oxidation to M(III), followed by decomposition. In case of the Bu^t substituent, the stereochemical rearrangement might be sufficiently slow so as to stabilize the M(II) derivatives, which ultimately can be characterized by ESR spectroscopy.

Mononuclear rhodium and iridium complexes with a d^7 electronic configuration are very uncommon.[16,23] In general, five-coordinate complexes are square pyramidal[16a,23] and four-coordinate complexes are square planar.[16b,c,23] The poor quality of the ESR spectra does not allow one to draw any structural conclusion for the Rh(II) and Ir(II) compounds reported in this paper. In light of the electrochemical data, however, one may reasonably conclude that these d^7 metal complexes also conform to the general trend of adopting a square planar coordination geometry.

Four analogous reasons, we cannot assign a precise stereochemistry to the Ir(0) and Rh(0) derivatives, although they should maintain a square-planar structure even though more or less pyramidalized as commonly found for four-coordinate rhodium and iridium with a d^9 electron configuration.[24]

Dioxygen and Carbon Monoxide Uptake. In the η^2-O_2 Ir(III) complexes of formula $[(PNalkyl)_2Ir(O_2)]^+$ (alkyl = Et, Pr^i), dioxygen is more strongly bound to the metal center than it is in the related rhodium compounds, in a sense that the latter complexes readily lose O_2 either upon bubbling nitrogen into their solutions or upon an increase in temperature.[4] The higher stability of the iridium complexes is consistent with the observed O–O bond distances, which are 1.47(1) Å in **7b**$^+$ and 1.436(9) Å in the rhodium complex $[(PNPr^i)_2Rh(O_2)]BPh_4$, recently authenticated by an X-ray analysis.[4] This finding is not surprising, as the larger radial extension of the $d\pi$ orbitals of iridium is expected to favor oxidative addition reactions which ultimately result in rather kinetically inert products. As a matter of fact, a few iridium complexes are known to efficiently assist oxygen-transfer reactions.[3c]

In the past, attempts have been made to correlate the O–O bond length of η^2-O_2 complexes and M–O bond strength with the degree of reversibility of their formation reactions.[3f,25] In view of a number of anomalous experimental data, the validity of such a correlation is now considered highly questionable;[3g] *e.g.*, the "irreversible" dioxygen adduct **7b**$^+$ and the "reversible" adduct $IrCl(PPh_2Et)_2(CO)(O_2)$ exhibit almost identical O–O distances.[26] In particular, it is generally agreed that correlation of O–O distances between metal complexes having significantly different ligands or containing chelate ring strain must be made with extreme caution.[3g,26-28]

For comparable complexes, it is observed that a high electron density at the metal favors the binding of dioxygen and its reduction to a peroxide form. As an example, in the well-known series of Vaska's dioxygen complexes $IrL_2(CO)X(O_2)$, the binding of O_2 becomes less irreversible and the O–O distance decreases as the auxiliary ligands become more electron releasing (L = $PPh_2Et > PPh_3$; X = I > Br > Cl).[3f] Valuable comparisons can also be made between complexes differing only in the nature of the metal center; for transition metals in the same periodic group, the stability of the dioxygen adducts increases in the order third-row > second-row, which is consistent with the results presented in this paper.[3f,g,29]

The electrochemical data reported in Table 4 preclude the fact that the formation of the dioxygen adducts of formula $[(PNalkyl)_2Ir(O_2)]^+$ (alkyl = Et, Pr^i) proceeds *via* an outer-sphere oxidation of the starting Ir(I) complexes to give Ir(III) species and O_2^{2-}, followed by their combination. On the other hand, the reaction of square-planar d^8 metal complexes with dioxygen to give η^2-O_2 adducts has a number of precedents.[3f,30] It is generally agreed that (i) the starting complexes distort in such a way as to destabilize the d_{xz} orbital sufficiently to allow an overlap with the π_g^* orbital of dioxygen[30a] and (ii) the kinetic barrier to the change of spin of molecular oxygen (triplet ground state) is circumbented by the reaction with the heavy transition metals (4d or 5d, as in the cases at hand).[3a]

Unlike the reactions with O_2, reactions of **1a**$^+$–**c**$^+$ and **2a**$^+$–**c**$^+$ with CO lead to reversible adducts. These complexes readily lose CO in solution, thus showing a lower affinity for carbon monoxide than for O_2. It is worthy of note that this is just the opposite of what happens in heme-iron proteins.[31]

The lack of strong binding of CO in square-planar d^8 complexes is not surprising in light of their stereochemical rigidity, which leads to the formation of square-pyramidal adducts. Actually, the interaction of CO with a square-planar d^8-metal complex is expected to be weak because of the repulsive effect of the filled d_{z^2} metal orbital.[21a]

Neither $[(PNBu^t)_2Ir]^+$ nor $[(PNBu^t)_2Rh]^+$ [4] binds dioxygen or carbon monoxide even at low temperature, suggesting that the steric hindrance of the ligands, and therefore the dimensions of the cavity available at the metal, play a critical role in the interaction with small molecules.

Acknowledgment. Thanks are expressed to the Progetti Finalizzati Chimica Fine II, CNR, Rome, for financial support and to Mr. Dante Masi for technical assistance in the X-ray crystal structure determination.

Supplementary Material Available: Tables S1 and S2, listing hydrogen atom locations and a complete set of crystallographic data for **7b**$^+$ (2 pages). Ordering information is given on any current masthead page.

(22) Marxen, T. L.; J. Johnson, B.; Nilsson, P. V.; Pignolet, L. H. *Inorg. Chem.* **1984**, *23*, 4663.
(23) (a) Serpone, N.; Jamieson, M. A. In *Comprehensive Coordination Chemistry*; Wilkinson, G., Gillard, R. D., McCleverty, J. A., Eds.; Pergamon Press: Oxford, England, 1987; Vol. 4, p 1120. (b) Dunbar, K. R.; Haefner, S. C. *Organometallics* **1992**, *11*, 1431. (c) Hay-Motherwell, R. S.; Koschmieder, S. U.; Wilkinson, G.; Hussain-Bates, B.; Hursthouse, M. B. *J. Chem. Soc., Dalton Trans.* **1991**, 2821. (d) Bianchini, C.; Peruzzini, M.; Laschi, F.; Zanello, P. In *Topics in Physical Organometallic Chemistry*; Gielen, M. F., Ed.; Freund Publishing House: London, 1992; Vol. 4, p 139. (e) Zecchin, S.; Zotti, G.; Pilloni, G. *J. Organomet. Chem.* **1985**, *294*, 379.
(24) (a) Serpone, N.; Jamieson, M. A. In *Comprehensive Coordination Chemistry*; Wilkinson, G., Gillard, R. D., McCleverty, J. A., Eds.; Pergamon Press: Oxford, England, 1987; Vol. 4, p 1100. (b) Jardine, F. H.; Sheridan, P. S. *Ibid.*, p 905.
(25) Vaska, L.; Chen, L. S.; Senoff, C. V. *Science* **1971**, *174*, 587.
(26) Weinnger, M. S.; Taylor, I. F., Jr.; Amma, E. L. *Chem. Commun.* **1971**, 1172.
(27) Shaw, B. L.; Stainbank, R. E. *J. Chem. Soc., Dalton Trans.* **1972**, 223.
(28) Gosh, A. G.; Terry, N. W.; Amma, E. L. *Trans. Am. Crystallogr. Assoc.* **1973** (Winter Meeting), 40.
(29) Vaska, L.; Chen, L. S.; Miller, W. V. *J. Am. Chem. Soc.* **1971**, *93*, 6671.
(30) (a) Gubelmann, M. H.; Williams, A. F. *Struct. Bonding (Berlin)* **1983**, *55*, 1. (b) Sakaki, S.; Hori, K.; Ohyoshi, A. *Inorg. Chem.* **1978**, *17*, 3183.
(31) Ochiai, E. *Bioinorganic Chemistry*; Allyn and Bacon: Boston, MA, 1977. See also references therein.